Inorganic Chemistry

ARTICLE

pubs.acs.org/IC

Self-Assembled β-$NaGdF_4$ Microcrystals: Hydrothermal Synthesis, Morphology Evolution, and Luminescence Properties

Fei He, Piaoping Yang,* Dong Wang, Na Niu, Shili Gai, and Xingbo Li

Key Laboratory of Superlight Materials and Surface Technology, Ministry of Education, and College of Material Science and Chemical Engineering, Harbin Engineering University, Harbin 150001, P.R. China

ABSTRACT: A self-assembly process has been designed for the controlled synthesis of β-$NaGdF_4$ with uniform morphology, dimension, and considerable monodispersity under a gentle hydrothermal condition using sodium citrate as the chelating agent. X-ray diffraction (XRD), scanning electron microscopy (SEM), transmission electron microscopy (TEM), high-resolution transmission electron microscopy (HRTEM), energy-dispersive X-ray spectrum (EDS), and up-conversion (UC) photoluminescence spectra were used to characterize the samples. The results indicate that the $NaGdF_4$ microcrystal can be rationally modified in phase, size, and morphology through tuning the pH value, sodium citrate content, and reaction time. Moreover, the hybrid process of the crystal growth and the self-assembly were thoroughly discussed, and a possible formation mechanism was proposed. Furthermore, the UC luminescence properties as well as the emission mechanisms of β-$NaGdF_4$:17%Yb^{3+}/3%Ln^{3+} (Ln = Er, Tm, Ho) microcrystals were systematically investigated. It is found that under 980 nm excitation, only limited emission bands were discovered which can be attributed to the energy gap and migration function of the Gd^{3+} ions in the β-$NaGdF_4$ microcrystals. It is expected that the synthetic strategy can be applied to prepare many other types of micro- and nanocrystals as well.

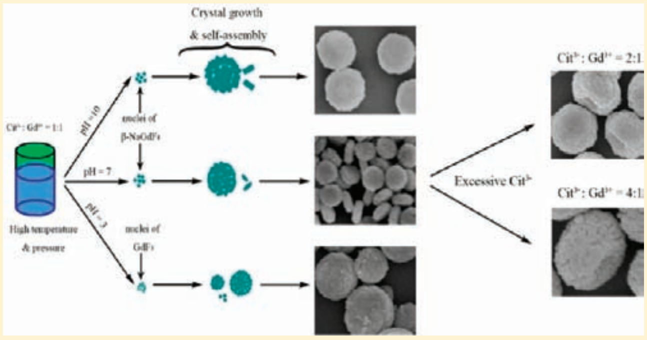

1. INTRODUCTION

In modern chemistry and materials science, controlled synthesis of well-defined inorganic micro- and nanocrystals (MCs and NCs) with uniform dimensions and shapes have become the hot spot of worldwide research because the electronic structure, bonding, surface energy, and chemical reactivity are directly related to their surface morphology.[1] Many methodologies including molten-salt method, hydrothermal process, template synthesis, and high boiling solvents method have been employed widely for the synthesis of a large range of nanostructures.[2−7] Among these routes, the hydrothermal method is capable of preparing different structured materials with high crystallinity and wide dimensions as long as chemicals and modifiers are correctly selected.[8−10] As a typical solution-based approach, this method has been proven to be an environmentally acceptable process with relatively high yield of desired products. Furthermore, it has been widely recognized that the crystal growth process is not only determined by its intrinsic structure but also significantly influenced by a series of external parameters, such as pH value, reaction time, and the chelating agent. In particular, the addition of special chelating agent, which has a significant effect on the kinetics of the crystal growth, has been demonstrated to be an effective strategy to achieve control over the morphology of final products.[11−13] Because of the high thermal stability and ability to form complexes with other metal ions, the citrate ions (Cit^{3-}) has the dynamic effect as a ligand and shape modifier by adjusting the growth rate of different facets under hydrothermal conditions, resulting in the formation of various geometries of the final products.[14−17]

Recently, rare earth materials have attracted much attention because of their unique electronic and optical properties based on their 4f electrons.[18−24] Particularly, because of their special advantages such as high light penetration depth in tissues, less photodamage to living organisms, low background light, and high sensitivity for detection, the up-conversion (UC) phosphors are of great potential in biological labeling and imaging technology, optical telecommunication, laser, medical diagnostics, and infrared quantum counters.[25−31] As a famous host material, the $NaREF_4$ (RE = rare earth) phosphors with some distinct advantages owing to the very low phonon frequencies have aroused intensive research in the past decades.[21−23,32,33] One example for this class of fluoride compounds is $NaGdF_4$, which is an ideal UC host material. Because the lowest excited level ($^6P_{7/2}$) of Gd^{3+} is situated in the ultraviolet region, which is far higher than most excited level of Yb^{3+} and Er^{3+} involved in the UC processes, the excitation energy loss through energy transfer from Yb^{3+} and Er^{3+} to the 4f level of Gd^{3+} can be avoided.[28,34] Moreover, the Gd^{3+} ions can act as an intermediate through which the excited energy can migrate over the Gd^{3+} sublattice and consequently facilitate the energy transfer process in fluoride

Received: January 23, 2011
Published: April 06, 2011

phosphor.[35] Recently, several methods have been developed to prepare the hexagonal β-phase $NaREF_4$ by involving the $NaGdF_4$ as the dopant.[36,37] Compared with the cubic α-phase structure, the hexagonal phase $NaREF_4$ is more stable and displays approximately one or two orders higher UC efficiency, especially in bulk materials and large-size particles.[38] Furthermore, the formation energy per atom in hexagonal phase increases by about 0.07 eV when Y^{3+} is replaced by Gd^{3+},[28] indicating that $NaGdF_4$ is more energetically stable than $NaYF_4$ in hexagonal phase and has longer luminescence lifetime as UC host material. However, compared with the $NaYF_4$ NCs which have been a research focus in the RE fluoride compounds, relatively less attention were paid in the $NaGdF_4$ NCs.

Up to now, some synthetic routes have been developed to selectively prepare the $NaGdF_4$ NCs. Boyer et al.[39] and Naccache et al.[40] prepared $NaGdF_4$ through the thermal decomposition synthesis route. The as-synthesized products are composed of single crystallites with uniform size distribution. However, demanding high temperature condition, low yield ratio, and the organic solvent involved in this method have limited its further application. Besides, there is still little work on the synthesis of $NaGdF_4$ MCs with well-defined shapes and good uniformity relative to the numerous effort on the $NaYF_4$ MCs.[3,41] Mech et al.[42] synthesized the hexagonal $NaGdF_4$:Eu^{3+} with average grain sizes of 20 nm from solution by a coprecipitation method. Zhang et al.[43] prepared both cubic and hexagonal $NaGdF_4$:Ce^{3+} as well as (Ce, Gd)F_3 MCs by controlling different molar ratio of reactants and synthesis temperatures through the hydrothermal procedure. Unfortunately, the morphology of as-prepared NCs is not uniform and the crystal growth process is still not given. Inorganic MCs with novel morphologies are of special significance in understanding the growth behavior and the potential technological applications in microelectronic devices. Therefore, $NaGdF_4$ phosphors with uniform novel morphology and high monodispersity synthesized by a facile and environmental friendly method are still desirable.

In the present work, we describe a template-free, no-seed, and aqueous-phase process for the synthesis of uniform β-$NaGdF_4$ MCs co-doped with Yb^{3+}/Ln^{3+} (Ln^{3+} = Er^{3+}, Tm^{3+}, Ho^{3+}) with high monodispersity via a facile and mild hydrothermal process. Sodium citrate was introduced into the reaction system to govern and adjust the morphology of the products. The effects of the molar ratio of sodium citrate to RE^{3+}, pH value of the initial solution, and reaction time on the crystal morphology have been investigated in detail. A possible mechanism of crystal growth has also been proposed. Additionally, the UC luminescence properties of Yb^{3+}/Er^{3+}, Yb^{3+}/Tm^{3+}, and Yb^{3+}/Ho^{3+} have been thoroughly studied in the obtained β-$NaGdF_4$ MCs.

2. EXPERIMENTAL SECTION

2.1. Materials. All materials including analytical grade $NaFB_4$, trisodium citrate, and NaOH were purchased from Sinopharm Chemical Reagent Co., Ltd. and used as received without further purification. 0.2 M Rare earth chloride stock solutions were prepared by dissolving the corresponding Gd_2O_3, Yb_2O_3, Er_2O_3, Tm_2O_3, Ho_2O_3 (99.99%, Changchun Applied Chemistry Science and Technology Limited, China) in hydrochloric acid at elevated temperature. All of the doping ratios of Ln^{3+} are in mole equivalents in our experiments.

2.2. Preparation of β-$NaGdF_4$. In a typical procedure for the synthesis of β-$NaGdF_4$, 5 mL of $GdCl_3$ (0.2 mol/L) was added into 10 mL of aqueous solution containing 1 mmol of trisodium citrate (labeled as Cit^{3-}) to form the metal-Cit^{3-} complex (1:1 molar ratio for Cit^{3-}/Gd^{3+}).

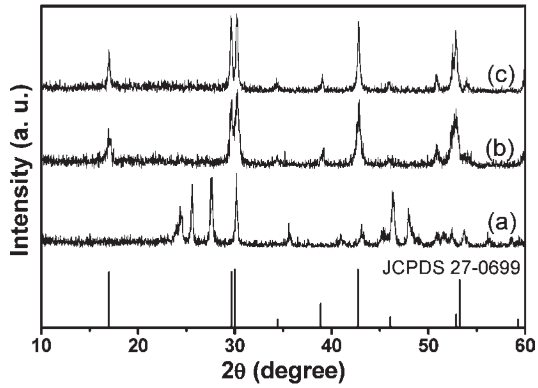

Figure 1. XRD patterns of $NaGdF_4$ MCs prepared at 180 °C for 24 h and pH values of 3 (a), 7 (b), and 10 (c). All of the samples were hydrothermally obtained with Cit^{3-}/Gd^{3+} molar ratios of 1:1.

Table 1. Unit Cell Lattice Constants and Crystallite Sizes for Orthorhombic Phase GdF_3 and Hexagonal β-$NaGdF_4$ Prepared at the pH Values of 3, 7, and 10, Respectively

samples	a (nm)	c (nm)	cell volume (nm^3)	crystallite size (nm)
JCPDS 49-1804	0.6571		0.20146	
GdF_3 (pH = 3)	0.6568	0.3601	0.20112	27.7
JCPDS 27-0699	0.6020		0.11302	
β-$NaGdF_4$ (pH = 7)	0.6018	0.3607	0.11374	19.3
β-$NaGdF_4$ (pH = 10)	0.6024	0.3606	0.11368	21.3

After vigorous stirring for 30 min, 3.125 mmol of $NaBF_4$ (12.5 mmol F^-) was added into the above solution. The pH of the mixture was adjusted to 7 by adding 1 mol/L NaOH. After additional agitation for 15 min, the as-obtained mixing solution was transferred into a Teflon bottle held in a stainless steel autoclave, which was sealed and maintained at 180 °C for 24 h. As the autoclave was naturally cooled to room temperature, the pH value of the solution was measured to be 3.58. Subsequently, the precipitates at the bottom were separated by centrifugation, washed with deionized water and ethanol in sequence, and then dried in air at 80 °C for 12 h. Other samples were prepared by a similar procedure, except for different pH values, Cit^{3-}/Gd^{3+} molar ratio, and reaction time. UC luminescent $NaGdF_4$:17% Yb^{3+}/3% Er^{3+}, $NaGdF_4$:17% Yb^{3+}/ 3% Tm^{3+}, and $NaGdF_4$:17% Yb^{3+}/ 3% Ho^{3+} samples were prepared in a manner similar to that for pure $NaGdF_4$ sample, which was prepared with pH value of 7 at 180 °C for 24 h.

2.3. Characterization. Powder X-ray diffraction (XRD) measurements were performed on a Rigaku-Dmax 2500 diffractometer at a scanning rate of 15°/min in the 2θ range from 10° to 60°, with graphite-monochromatized Cu Kα radiation (λ = 0.15405 nm). SEM images were obtained using a field emission electron microscope (FESEM, S4800, Hitachi) equipped with an energy-dispersive X-ray spectrum (EDS, JEOL JXA-840). Transmission electron microscopy (TEM) and high-resolution transmission electron microscopy (HRTEM) were performed on a FEI Tecnai G^2 S-Twin instrument with a field emission gun operating at 200 kV. Images were acquired digitally on a Gatan multiple CCD camera. The UC emission spectra were obtained using a 980 nm laser from an OPO (optical parametric oscillator, Continuum Surelite, U.S.A.) as the excitation source and detected by a photomultiplier tube (HAMAMATSU R955) from 400 to 900 nm. All the measurements were performed at room temperature.

3. RESULTS AND DISCUSSION

3.1. Phase, Structure, and Morphology. In the previous reports for the synthesis of the RE fluoride, some necessary conditions have been proposed to investigate the changes of the products in different reaction systems.[44,45] Figure 1 exhibits XRD patterns of the as-synthesized samples using $NaBF_4$ as fluoride source under various pH conditions. The regularity indicated from the results is described as follows. For the sample prepared at pH value of 3 (Figure 1a), the diffraction peaks display the presence of orthorhombic GdF_3 phase (JCPDS 49-1804), while pure hexagonal β-phase $NaGdF_4$ indexed to the standard data (JCPDS 27-0699) can be obtained under the pH value of 7 (Figure 1b) and 10 (Figure 1c). The calculated cell lattice constants of the samples prepared at different pH values are summarized in Table 1, the standard data (JCPDS 49-1804) for orthorhombic GdF_3 and the standard data (JCPDS 27-0699) for hexagonal β-$NaGdF_4$ are also given for comparison. Obviously, the calculated cell lattice constants are consistent with the standard data, implying the high crystallinities. The main reason for the formation of different phases is that $NaBF_4$ can slowly hydrolyze to produce HF and H_3BO_3 in the aqueous solution, as shown in eq 2.[46,47] In an acid environment (pH = 3), this situation is not favorable for the release of F^- from the reaction equilibrium. On the contrary, the molar amounts of F^- and Na^+ ions will gradually turn equal with the rising of the pH value in the reaction system. In this case, Gd^{3+} released from the complexes reacts with abundant F^- and Na^+ to form the crystal nuclei of $NaGdF_4$. As can be seen from the reaction, corresponding H^+ are produced, and the solution become acidic, which is in good accordance with the change of pH value in the Experimental Section. Further growth of the particle and the self-assembly process will be discussed subsequently. The possible reaction process for the formation of the $NaGdF_4$ crystal nuclei can be summarized as follows:

$$Gd^{3+} + Cit^{3-} \rightarrow Gd^{3+}{-}Cit^{3-}\ (\text{complex}) \tag{1}$$

$$BF_4^- + 3H_2O \leftrightarrow 3HF + F^- + H_3BO_3 \tag{2}$$

$$2H_3BO_3 + Na^+ \rightarrow Na_2B_2O_4 + 2H_2O + 2H^+ \tag{3}$$

$$Na^+ + Gd^{3+}{-}Cit^{3-} + 4F^- \rightarrow NaGdF_4 + Cit^{3-} \tag{4}$$

In addition, the diffraction peaks of these samples show some broadening, which indicates the fine nature of the crystallinity in those samples. The peak broadening was used to calculated the crystallite sizes by the Scherrer formula, $D = 0.89\lambda/\beta \cos \theta$, where D is the average grain size, λ is the X-ray wavelength (0.154505 nm), and β and θ are the diffraction angle and full-width at half-maximum (fwhm), respectively. As shown in Table 1, the calculated average crystallite sizes for the samples prepared at the pH value of 3, 7, and 10 are 27.7 (GdF_3), 19.3 and 21.3 nm ($NaGdF_4$), respectively.

Figure 2 displays the SEM, TEM, HRTEM images, and EDS spectrum of the typical $NaGdF_4$ MCs prepared with pH value of 7 and Cit^{3+}/Gd^{3+} molar ratio of 1:1 at 180 °C for 24 h. It can be seen from Figure 2a that the $NaGdF_4$ MCs exhibit uniform and hierarchical oblate microspheres with a mean diameter of 600 nm. These MCs exhibit considerable monodispersity and narrow size distribution. As can be seen from the high-magnification SEM image (Figure 2b), the uniform oblate spheroids with the thickness of about 150 nm are multilayer and self-assembled with the unit-particles. The typical TEM image shows the

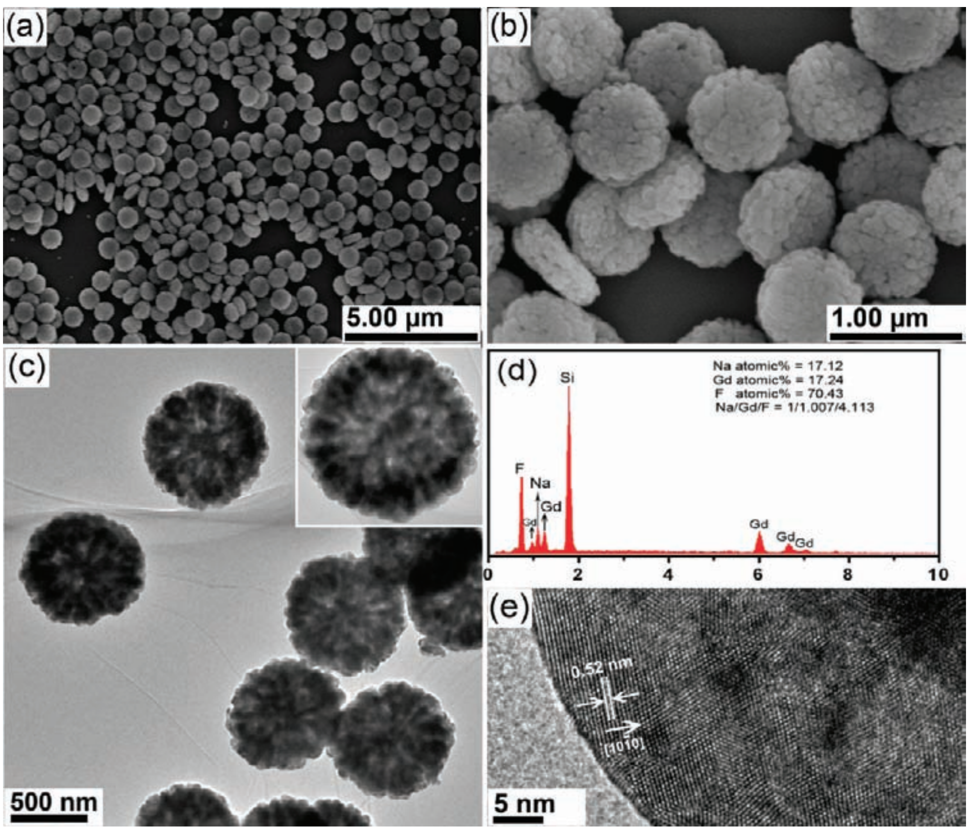

Figure 2. Low-magnification FE-SEM image (a), high-magnification FE-SEM image (b), TEM image (c), EDS (d), and HRTEM image (e) of $NaGdF_4$ MCs (Cit^{3-}/Gd^{3+} = 1:1) prepared at pH value of 7 and 180 °C for 24 h.

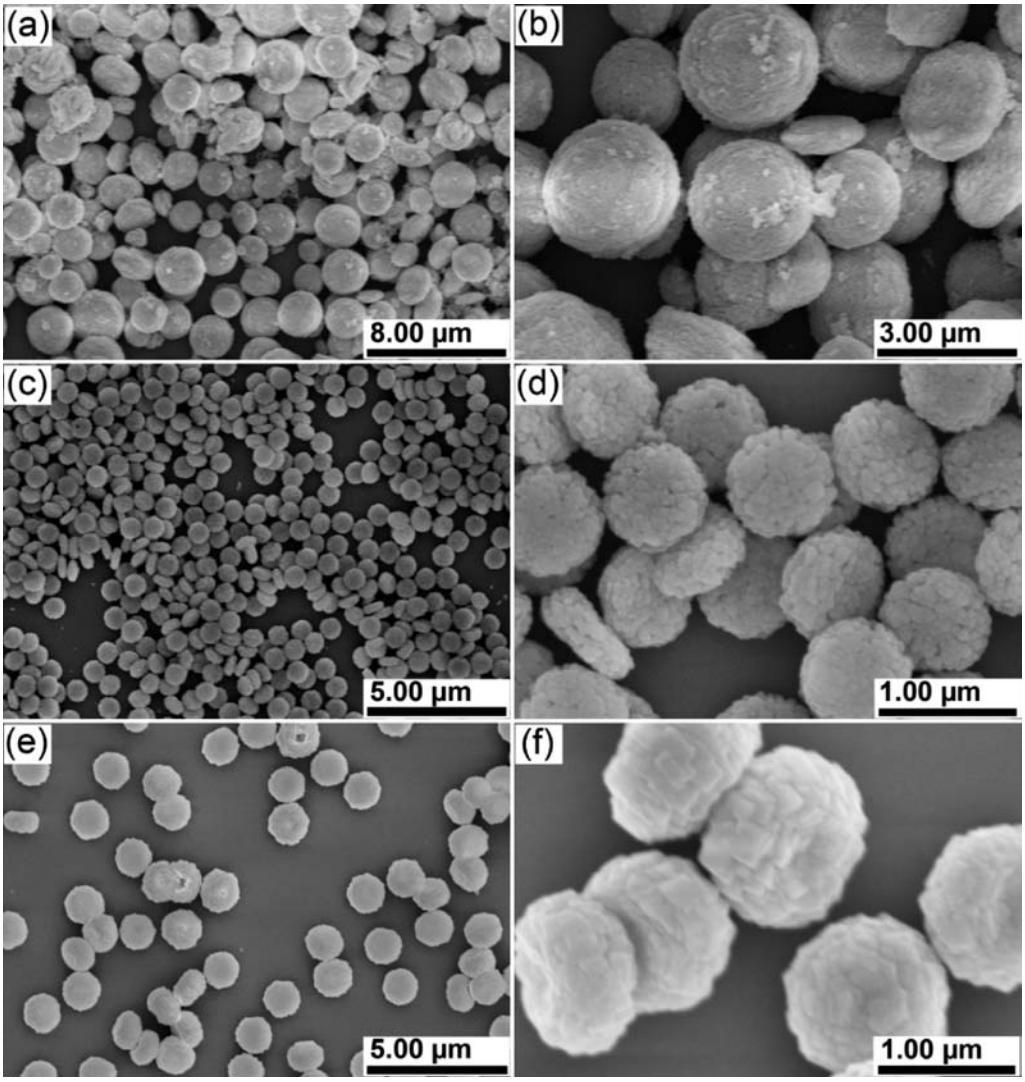

Figure 3. SEM images of $NaGdF_4$ MCs prepared at 180 °C for 24 h and pH values of 3 (a, b), 7 (c, d), and 10 (e, f). All of the samples were hydrothermally obtained with Cit^{3-}/Gd^{3+} molar ratios of 1:1.

obvious spherical microstructure with a uniform size distribution (Figure 2c). It should be noted that the fringe of oblate spheroid is much thicker than the center (inset in Figure 2c), also indicating the possible self-assembly process. From the EDS analysis in Figure 2d, it confirms the presence of Na, Gd, and F (Si from the Si substrate), and the atomic ratio of Na/Gd/F is 1/1.007/4.113, which is in great agreement with the theoretical atomic Na/Gd/F ratio (1/1/4). A polycrystalline structure can be clearly found from the HRTEM image (Figure 2e), and the interplanar distance between adjacent lattice planes (marked by the arrows) is about 0.52 nm, which corresponds well to the value of the $[10\bar{1}0]$ planes of the hexagonal $NaGdF_4$ phase.

3.2. Influential Factors and Possible Formation Mechanism. In the following sections, the effects of pH values in the initial solution, Cit^{3-} content, and reaction time on the crystal structures and shapes of final products have been investigated in detail. Moreover, the possible formation mechanism for β-$NaGdF_4$ MCs with various morphologies is presented.

Effect of pH Values. To investigate effect of pH values on the morphology of $NaGdF_4$ MCs, a series of contrast experiments were conducted. Figure 3 shows the low and high-magnification SEM images of $NaGdF_4$ MCs synthesized at 180 °C for 24 h with various pH values, while keeping the Cit^{3-}/Gd^{3+} molar ratio of 1/1. For the GdF_3 sample prepared at pH value of 3 (Figure 3a, 3b), the self-assembled, hierarchical oblate spheroid structure is discovered. Obviously, the dimension of the GdF_3 MCs is larger than that of the $NaGdF_4$ microcrystal (Figure 3c, 3d) which can be attributed to the character of orthorhombic phase of the GdF_3 growth as well as the relative speed between the crystal growth and self-assembly process. In fact, the differences of pH values exhibit a significantly effect on the existent form and complexing ability of Cit^{3-} to Gd^{3+}. In acidic condition, the Cit^{3-} would partly combine H^+ and exists as H_xCit^{x-3}, directly decreasing its complexing ability with metal ions to a great degree. Furthermore, the self-assembly process can be promoted by the strong hydrogen-bond in acidic solution.[48] So the speed of forming GdF_3 nuclei as well as the self-assembly process is higher than that of crystal growth, resulting in the larger crystal dimension. Furthermore, the inhomogeneous grain diameter of the product prepared at pH value of 3 implies a lack of equilibrium and equivalent speed of the self-assembly process, because of the lower pH value. When prepared at pH = 10 (Figure 3e, 3f), the

dx.doi.org/10.1021/ic200155q |Inorg. Chem. 2011, 50, 4116–4124

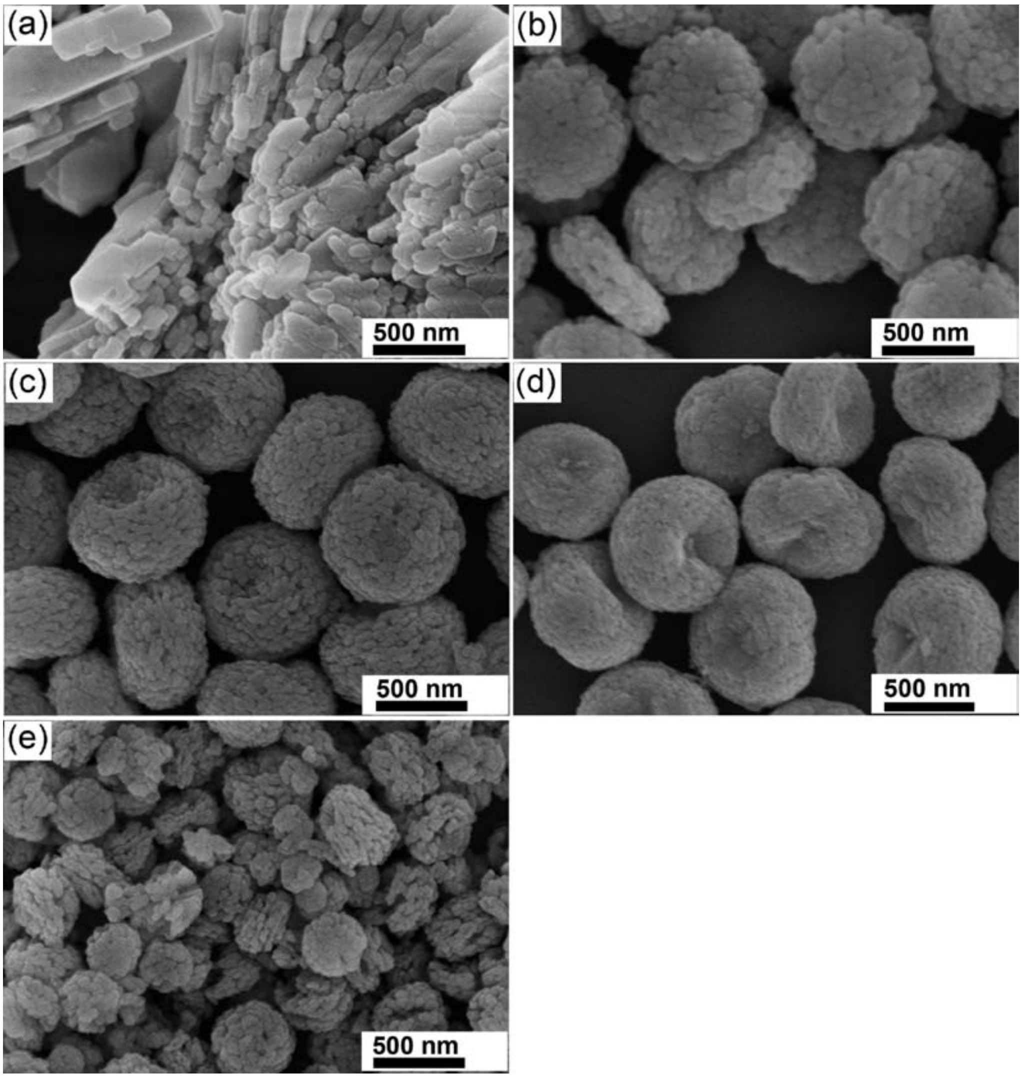

Figure 4. SEM images of $NaGdF_4$ MCs prepared with different Cit^{3-}/Gd^{3+} molar ratios. 0 (without sodium citrate) (a), 1:1 (b), 2:1 (c), 4:1 (d), and 8:1 (e). All of the samples were hydrothermally obtained at 180 °C for 24 h with the pH value of the initial solution kept at 7.

component monomers of the $NaGdF_4$ MCs exhibit larger size compared with the sample prepared at the pH value of 7 (Figure 3c, 3d, discussed previously). Owing to the strengthening repulsive electrostatic interaction of the Gd^{3+} ions with the increasing pH value,[49] the self-assembly process is restrained; thus, the components can grow further.

Effect of Sodium Citrate Content. The SEM images (Figure 4) provide the size and shapes of the $NaGdF_4$ MCs synthesized with different Cit^{3-}/Gd^{3+} molar ratio. All of the samples were hydrothermally obtained at 180 °C for 24 h with the pH value of the initial solution kept at 7. For β-$NaGdF_4$ obtained without sodium citrate (Figure 4a), the crystals tend to grow into irregular structures and aggregate in the form of disorder. However, once sodium citrate is introduced into the reaction system, significant change takes place in the morphology of crystals. Figure 4b shows the SEM image of the sample synthesized with Cit^{3-}/Gd^{3+} molar ratio of 1/1. It can be seen that the crystals were assembled with uniform components and exhibit regular oblate spheroid morphology and considerable monodispersity. This indicates that the citrate anions have a significant role in the formation of the β-$NaGdF_4$ MCs structure. Although the mechanism for the change of crystal morphology grown with and without sodium citrate has been discussed before,[50,51] and the relative rates of growth along different crystallographic directions controlled by the Cit^{3-} ions are always introduced to explain the different outlook of the crystallite.[52,53] However, this mechanism has been only demonstrated in the systems with a single process of crystal growth. In the present system, crystal growth and self-assembly coexist. So the effect of Cit^{3-} ions on the crystal morphology should be illustrated from both sides. In the initial solution, a stable $Gd^{3+}-Cit^{3-}$ complex was formed. Then the hydrolysis of the complex produced colloidal sol under high temperature and pressure, where the $NaGdF_4$ nuclei were covered with Cit^{3-}, and these molecules adsorbed on the surface of the particles formed a protective layer to hold back the further growth of particles. However, because of the anisotropy of the β-phase $NaGdF_4$, the inhibitory action is heterogeneous to different planes and, consequently, the nearly oval structure (pH = 7) as well as the laminar structure (pH = 10) were discovered. As for self-assembly process, the Cit^{3-} plays an important role in providing the H-bonding and cross-linking between the $NaGdF_4$ particles. As its content rises (Figure 4c, 4d), the Cit^{3-} ions acts

dx.doi.org/10.1021/ic200155q | *Inorg. Chem.* 2011, 50, 4116–4124

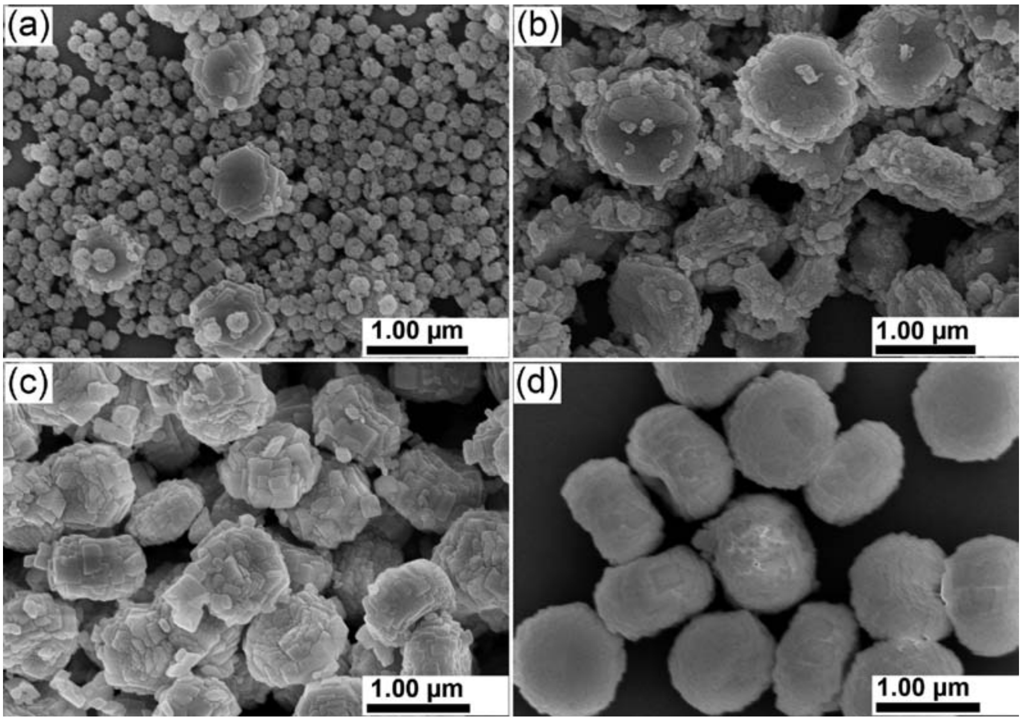

Figure 5. SEM images of $NaGdF_4$ MCs (Cit^{3-}/Gd^{3+} = 1:1) synthesized at 180 °C for different reaction time. 2 h (a), 6 h (b), 12 h (c), and 24 h (d). All of the samples were obtained with the initial pH value of 10.

Scheme 1. Schematic Illustration for the Formation Process of $NaGdF_4$ MCs Prepared at Different Conditions

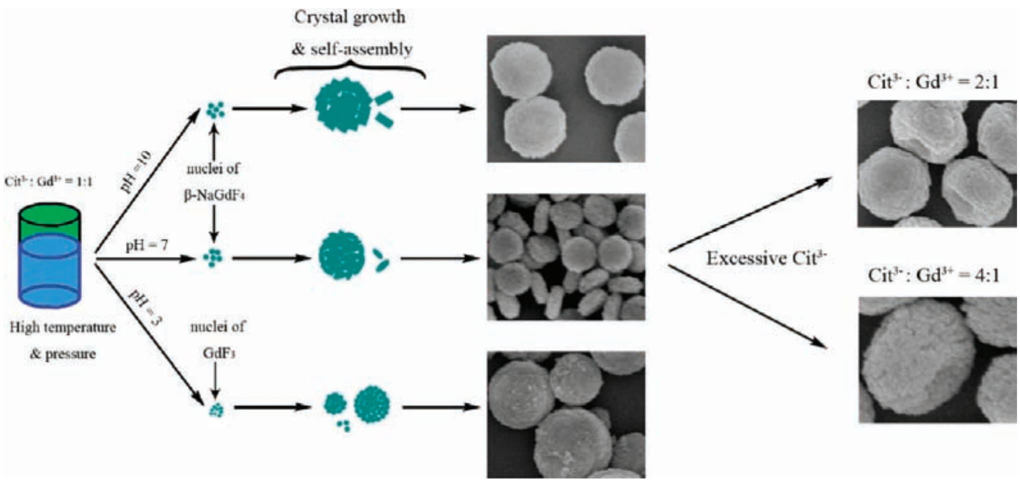

progressively more as the crystal growth depressant and cross-linking role. The component dimension reveals a trend of decrease, while the microcrystal structure shows further growth perpendicular to the orbicular side tendency. By further addition of the sodium citrate, the chelating effect of the Cit^{3-} is further enhanced. Besides, as a surfactant, the sodium citrate can also largely lower the surface energy of the particles. Therefore, the formation and growth of the initial nucleus is further reduced, and the self-assembly process of $NaGdF_4$ crystals is relatively promoted. Moreover, the surfaces of top/bottom have obvious concave centers, which suggest the low surface energy and the orientation of the self-assembly process. However, when the Cit^{3-}/Gd^{3+} molar ratio is increased to 8:1 (Figure 4e), the products become anomalously aggregated, which is probably due to the complex effect of the excessive Cit^{3-}. Although the exact function of Cit^{3-} on the formation of the $NaGdF_4$ MCs in our synthetic system is not yet fully understood, it is clearly that three main roles of the Cit^{3-} are responsible for the morphology. One is the strong selective adsorption growth depressant effect of Cit^{3-} on various planes of the particles. The other is the cross-linked role between the particles with H-bonding. And the last is the greatly lowered formation and surface energy, which promote the self-assembly process.

Effect of the Reaction Time. Because the final microcrystal structure of $NaGdF_4$ is formed by small components, the self-assembly process was investigated with a prolonged reaction time

dx.doi.org/10.1021/ic200155q |*Inorg. Chem.* 2011, 50, 4116–4124

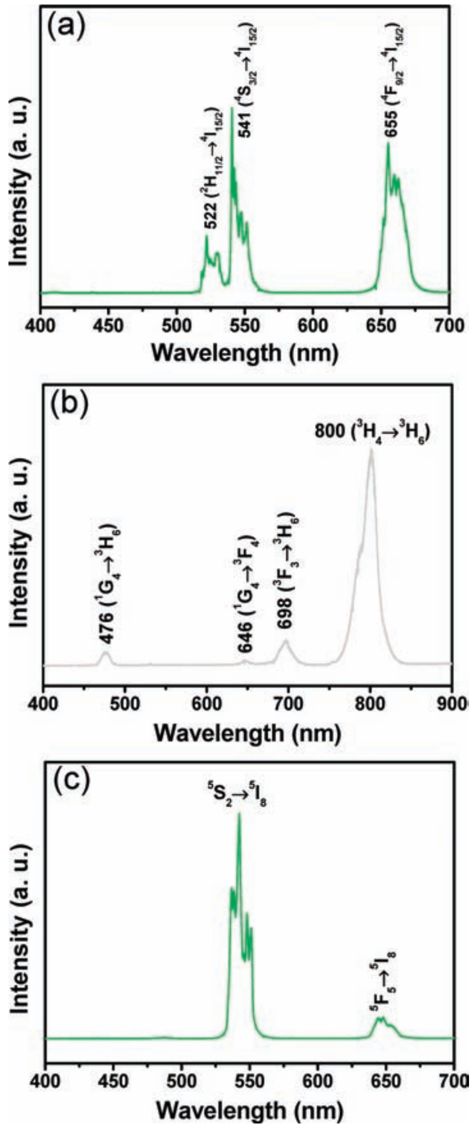

Figure 6. NIR-to-visible UC emission spectra of $NaGdF_4$:Yb/Er (a), $NaGdF_4$:Yb/Tm (b), and $NaGdF_4$:Yb/Ho (c) MCs under 980 nm laser excitation.

at the same pH value of 10 and hydrothermal temperature (180 °C). Figure 5 shows the SEM images of the $NaGdF_4$ samples prepared with 1:1 Cit^{3-}/Gd^{3+} at different reaction time. At t = 2 h, a typical SEM image (Figure 5a) reveals that the sample consists of a mass of particles with a particle size of about 160−180 nm and a small number of hierarchical laminar-assembled spheroids. The rough surface and the evident boundaries of the spheroids indicated that the spheroids are composed of many thin laminars, and these original laminars are self-assembled into an integrated structure along the longitudinal axis direction through face-to-face attachment. When the reaction time is prolonged to 6 and 12 h, the hierarchical oblate spheroids become the dominant morphology of the products, as shown in Figure 5b and Figure 5c. Moreover, careful observation indicates that the tiny components assembly increases gradually in size with the reaction proceeding. Interestingly, in this period, the components with grown size and sheet structure are assembled along the radial direction of spheroids. Further increasing the reaction time to 24 h, the oblate microcrystals with uniform diameter and considerable monodispersity are obtained. According to the above process, the growth and directed attachment of the $NaGdF_4$ nanoparticles can be distinctly observed, which visually demonstrate the crystal growth and self-assembly process.[54,55]

On the basis of the above analysis, it can be inferred that, besides inherent unit cell structures of nucleated seeds, the Cit^{3-} contents, pH values in the initial solution, and reaction times are all important factors in the phase and morphology evolution of the final products. Scheme 1 summarizes the possible shape formation processes of different gadolinium related fluorides under various experimental conditions.

3.3. Up-Conversion Luminescence Properties of the Products. To investigate the UC luminescent properties of the β-$NaGdF_4$ host, 17% Yb^{3+} and 3% Ln^{3+} (Ln = Er, Tm, Ho) were added to form co-doped β-$NaGdF_4$:Yb^{3+}/Ln^{3+} crystals. Under 980 nm IR laser excitation, the strong yellowish-green, whitish, and green luminescence can be observed in the Yb^{3+}/Er^{3+}, Yb^{3+}/Tm^{3+}, and Yb^{3+}/Ho^{3+} ion-pair co-doped β-$NaGdF_4$ MCs, respectively. As shown in Figure 6a for β-$NaGdF_4$:Yb^{3+}/Er^{3+}, the emission bands centered at 522, 541, and 655 nm can be assigned to $^2H_{11/2}\rightarrow{}^4I_{15/2}$, $^4S_{3/2}\rightarrow{}^4I_{15/2}$, and $^4F_{9/2}\rightarrow{}^4I_{15/2}$ transitions of Er^{3+}, respectively.[36,56,57] The corresponding CIE coordinates for the emission spectra of β-$NaGdF_4$: Yb^{3+}/Er^{3+} are determined as x = 0.3216, y = 0.5852, located in the green region (point a, Figure 7). In Figure 6b for β-$NaGdF_4$:Yb^{3+}/Tm^{3+}, the four emission bands centered at 476, 646, 698, and 800 nm can be attributed to the $^1G_4\rightarrow{}^3H_6$, $^1G_4\rightarrow{}^3F_4$, $^3F_3\rightarrow{}^3H_6$, and $^3H_4\rightarrow{}^3H_6$ transitions of Tm^{3+}.[58−60] The corresponding CIE coordinates for the emission spectra are determined as x = 0.3067, y = 0.2879, located in the white region (point b, Figure 7). As for β-$NaGdF_4$:Yb^{3+}/Ho^{3+} in Figure 6c, predominantly green emission band centered at 542 nm is observed and corresponding to the $^5S_2\rightarrow{}^5I_8$ transition of Ho^{3+}.[40,61] The notably weaker red emission (relative to the green emission) band discovered at 648 nm is ascribed to the transition from the $^5F_5\rightarrow{}^5I_8$. The corresponding CIE coordinates for the emission spectra are determined as x = 0.3588, y = 0.5543, located in the green region (point c, Figure 7).

The proposed up-conversion mechanism in the β-$NaGdF_4$: Yb/Ln MCs is demonstrated in Figure 8. In the β-$NaGdF_4$ crystal lattice, Er^{3+}, Tm^{3+}, and Ho^{3+} do not have an energy level resonant with 980 nm, which corresponds to the excitation wavelength of the diode, suggesting that the up-conversion process is initiated by the first raising of Yb^{3+} ion to the $^2F_{5/2}$ excited-state via an incoming pump photon.[62] The subsequent step involves an energy transfer (ET) process, by which the energy levels of Er^{3+} $^4I_{11/2}$, Tm^{3+} $^3H_5$, and Ho^{3+} $^5I_6$ were excited. Meanwhile, some of the excited ions relax rapidly to the low-lying levels of the Er^{3+} $^4I_{13/2}$, Tm^{3+} $^3F_4$, and Ho^{3+} $^5I_7$ states. Once these states are populated, a subsequent incoming pump photon or a second ET from a neighboring Yb^{3+} ion may result in the population of the $^4F_{7/2}$, $^4F_{9/2}$, $^3F_2$, $^5F_5$ states of these ions. The population of these state may also occur via a nonradiative decay to the low-lying $^2H_{11/2}$ $^4S_{3/2}$ of the Er^{3+}, $^3F_2$ and $^3F_3$ of the Tm^{3+} as well as $^5I_4$ of the Ho^{3+}. Therefore, the emissions from these populated states to the ground states take place. Moreover, the Gd^{3+} ions in the ground state cannot absorb 980-nm photons or the energy in the populated states for the large energy gap between the first excited state and the ground state. Thus, superfluous energy consuming is forbidden, and the main emission discussed above can be enhanced.

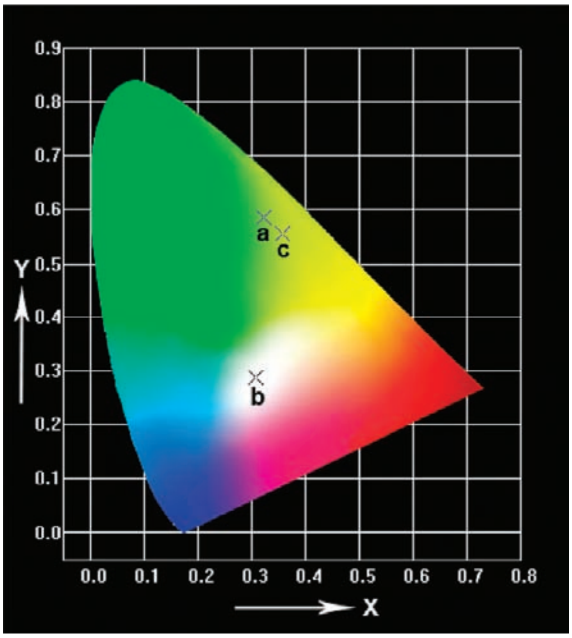

Figure 7. CIE chromaticity diagram showing the emission colors for $NaGdF_4$:Yb/Er (a), $NaGdF_4$:Yb/Tm (b), and $NaGdF_4$:Yb/Ho (c).

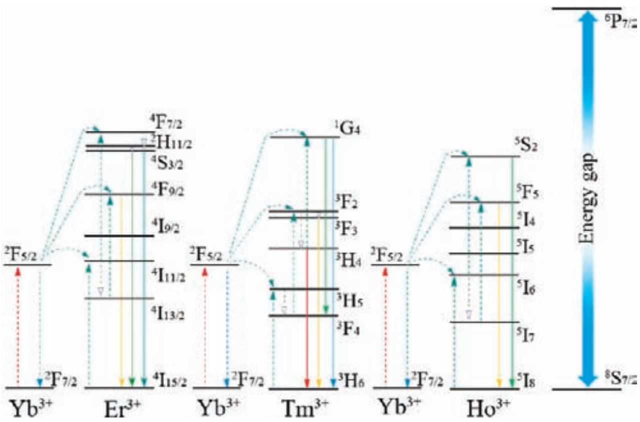

Figure 8. Proposed energy transfer mechanisms under 980-nm diode laser excitation in $NaGdF_4$:Yb/Er, $NaGdF_4$:Yb/Tm, and $NaGdF_4$:Yb/Ho, respectively.

4. CONCLUSIONS

In summary, the β-$NaGdF_4$ MCs were synthesized through a mild and manageable hydrothermal method by using the sodium citrate as the shape regulator. The results indicate that Cit^{3-} has significant role in the morphology of the products, and its effects will be strongly influenced by its content and the pH value of initial solution. In addition, the hydrolytic equilibrium was introduced to explain the formation of GdF_3 and $NaGdF_4$ nuclei, as well as the crystal growth and self-assembly processes. The possible formation mechanisms for GdF_3 and $NaGdF_4$ MCs with diverse morphologies were presented in detail. Furthermore, co-doped RE elements Yb^{3+}/Ln^{3+} (Ln = Er, Tm, Ho) exhibit characteristic emission properties respectively in the β-$NaGdF_4$ MCs host owing to the broad energy band and the migration function of the Gd^{3+} ions. The products with particular characteristics may have the promising potential to serve as versatile luminescent phosphors for further application.

■ AUTHOR INFORMATION

Corresponding Author
*E-mail: yangpiaoping@hrbeu.edu.cn.

■ ACKNOWLEDGMENT

This project is financially supported the National Natural Science Foundation of China (NSFC 20871035), China Postdoctoral Special Science Foundation (200808281), and Harbin Sci.-Tech. Innovation Foundation (No. 2009RFQXG045).

■ REFERENCES

(1) Li, H.; Liu, R.; Zhao, R.; Zheng, Y.; Chen, W.; Xu, Z. *Cryst. Growth Des.* **2006**, *6*, 2795.
(2) Zhou, H.; Mao, Y.; Wong, S. S. *Chem. Mater.* **2007**, *19*, 5238.
(3) Li, C.; Yang, J.; Quan, Z.; Yang, P.; Kong, D.; Lin, J. *Chem. Mater.* **2007**, *19*, 4933.
(4) Mao, Y.; Park, T.-J.; Zhang, F.; Zhou, H.; Wong, S. S. *Small* **2007**, *3*, 1122.
(5) Liu, Q. S.; Lu, W. G.; Ma, A. H.; Tang, J. K.; Lin, J.; Fang, J. Y. *J. Am. Chem. Soc.* **2005**, *127*, 5276.
(6) Liu, Q. S.; Yan, Z.; Henderson, N. L.; Bauer, J. C.; Goodman, D. W.; Batteas, J. D.; Schaak, R. E. *J. Am. Chem. Soc.* **2009**, *131*, 5720.
(7) Wang, Z. L.; Quan, Z. W.; Jia, P. Y.; Lin, C. K.; Luo, Y.; Chen, Y.; Fang, J.; Zhou, W.; O'Connor, C. J.; Lin *J. Chem. Mater.* **2006**, *18*, 2030.
(8) Wang, L. Y.; Li, Y. D. *Chem. Mater.* **2007**, *19*, 727.
(9) Huang, Y.; You, H.; Jia, G.; Zheng, Y.; Song, Y.; Yang, M.; Liu, K.; Zhang, L. *J. Phys. Chem. C* **2009**, *113*, 16962.
(10) Wang, W. W.; Yao, J. L. *J. Phys. Chem. C* **2009**, *113*, 3070.
(11) Jiang, D.; Li, J.; Xie, D.; Zhu, J.; Chen, M.; Lü, X.; Dang, S. *J. Colloid Interface Sci.* **2010**, *350*, 30.
(12) Sun, Y.; Xia, Y. *Adv. Mater.* **2002**, *14*, 833.
(13) Hou, Z.; Yang, P.; Li, C.; Wang, L.; Lian, H.; Quan, Z.; Lin, J. *Chem. Mater.* **2008**, *20*, 6686.
(14) Sun, Y.; Liu, H.; Wang, X.; Kong, X.; Zhang, H. *Chem. Mater.* **2006**, *18*, 2726.
(15) Hao, Q.; Xu, L.; Li, G.; Qian, Y. *Langmuir* **2009**, *25*, 6363.
(16) Kim, T.-U.; Kim, J.-A.; Pawar, S. M.; Moon, J.-H.; Kim, J. H. *Cryst. Grow Des.* **2010**, *10*, 4256.
(17) Zhang, C.; Li, C.; Peng, C.; Chai, R.; Huang, S.; Yang, D.; Cheng, Z.; Lin, J. *Chem.—Eur. J.* **2010**, *16*, 5672.
(18) Wang, J. W.; Tanner, P. A. *J. Am. Chem. Soc.* **2010**, *132*, 947.
(19) Tanner, P. A.; Fu, L. S.; Cheng, B. M. *J. Phys. Chem. C.* **2009**, *113*, 10773.
(20) Zhang, F.; Wan, Y.; Yu, T.; Zhang, F. Q.; Shi, Y. F.; Xie, S. H.; Li, Y. G.; Xu, L.; Tu, B.; Zhao, D. Y. *Angew. Chem., Int. Ed.* **2007**, *46*, 7976.
(21) Shi, D. L.; Lian, J.; Wang, W.; Liu, G. K.; He, P.; Dong, Z. Y.; Wang, L. M.; Ewing, R. C. *Adv. Mater.* **2006**, *18*, 189.
(22) Chelebaeva, E.; Larionova, J.; Guari, Y.; Ferreira, R. A. S.; Carlos, L. D.; Paz, F. A. A.; Trifonov, A.; Guérin, C. *Inorg. Chem.* **2009**, *48*, 5983.
(23) Kostova, M. H.; Ananias, D.; Paz, F. A. A.; Ferreira, A.; Rocha, J.; Carlos, L. D. *J. Phys. Chem. B* **2007**, *111*, 3576.
(24) Carlos, L. D.; Ferreira, R. A. S.; Pereira, R. N.; Assuncao, M.; Bermudez, V. D. *J. Phys. Chem. B.* **2004**, *108*, 14924.
(25) Heer, S.; Kömpe, K.; Güdel, H. U.; Haase, M. *Adv. Mater.* **2004**, *16*, 2102.
(26) Suyver, J. F.; Aebischer, A.; Biner, D.; Gerner, P.; Grimm, J.; Heer, S.; Krämer, K. W.; Reinhard, C.; Güdel, H. U. *Opt. Mater.* **2005**, *27*, 1111.
(27) Auzel, F. *Chem. Rev.* **2003**, *104*, 139–174.
(28) Wang, F.; Han, Y.; Lim, C. S.; Lu, Y.; Wang, J.; Xu, J.; Chen, H.; Zhang, C.; Hong, M.; Liu, X. *Nature* **2010**, *463*, 1061.
(29) Li, C.; Lin, J. *J. Mater. Chem.* **2010**, *20*, 6831.

(30) Zhang, C.; Ma, P.; Li, C.; Li, G.; Huang, S.; Yang, D.; Shang, M.; Kang, X.; Lin, J. *J. Mater. Chem.* **2011**, *21*, 717.

(31) Wu, Y.; Li, C.; Yang, D.; Lin, J. *J. Colloid Interface Sci.* **2011**, *354*, 429.

(32) Ptacek, P.; Schafer, H.; Kompe, K.; Haase, M. *Adv. Funct. Mater.* **2007**, *17*, 3843.

(33) Mai, H. X.; Zhang, Y. W.; Si, R.; Yan, Z. G.; Sun, L. D.; You, L. P.; Yan, C. H. *J. Am. Chem. Soc.* **2006**, *128*, 6426.

(34) Mahiou, R.; Arbus, A.; Cousseins, J. C.; Fournier, M. T. *J. Less—Common Met.* **1987**, *136*, 9.

(35) Blasse, G. *Mater. Chem. Phys.* **1987**, *16*, 201.

(36) Guo, H.; Li, Z. Q.; Qian, H. S.; Hu, Y.; Muhammad, I. N. *Nanotechnology* **2010**, 21.

(37) Abel, K. A.; Boyer, J.-C.; van Veggel, F. C. J. M. *J. Am. Chem. Soc.* **2009**, *131*, 14644.

(38) Yi, G. S.; Chow, G. M. *Adv. Funct. Mater.* **2006**, *16*, 2324.

(39) Boyer, J.-C.; Gagnon, J.; Cuccia, L. A.; Capobianco, J. A. *Chem. Mater.* **2007**, *19*, 3358.

(40) Naccache, R.; Vetrone, F.; Mahalingam, V.; Cuccia, L. A.; Capobianco, J. A. *Chem. Mater.* **2009**, *21*, 717.

(41) Li, C.; Quan, Z.; Yang, J.; Yang, P.; Lin, J. *Inorg. Chem.* **2007**, *46*, 6329.

(42) Mech, A.; Karbowiak, M.; Kepinski, L.; Bednarkiewicz, A.; Strek, W. *J. Alloys Compd.* **2004**, *380*, 315.

(43) Zhang, X. Q.; Fan, X. P.; Qiao, X. S.; Luo, Q. *Mater. Chem. Phys.* **2010**, *121*, 274.

(44) Li, C.; Yang, J.; Yang, P.; Lian, H.; Lin, J. *Chem. Mater.* **2008**, *20*, 4317.

(45) Li, C.; Quan, Z.; Yang, P.; Huang, S.; Lian, H.; Lin, J. *J. Phys. Chem. C.* **2008**, *112*, 13395.

(46) Miao, Z. J.; Liu, Z. M.; Ding, K. L.; Han, B. X.; Miao, S. D.; An, G. M. *Nanotechnology* **2007**, *18*, 125605.

(47) Zhu, L.; Meng, J.; Cao, X. *Eur. J. Inorg. Chem.* **2007**, *2007*, 3863.

(48) Sun, Z. H.; Ni, W. H.; Yang, Z.; Kou, X.; Li, L.; Wang, J. F. *Small* **2008**, *4*, 1287.

(49) Si, S.; Raula, M.; Paira, T. K.; Mandal, T. K. *ChemPhysChem* **2008**, *9*, 1578.

(50) Li, W.-J.; Shi, E.-W.; Zhong, W.-Z.; Yin, Z.-W. *J. Cryst. Growth* **1999**, *203*, 186.

(51) Laudise, R. A.; Ballman, A. A. *J. Phys. Chem.* **1960**, *64*, 688.

(52) Laudise, R. A.; Kolb, E. D.; Caporaso, A. J. *J. Am. Chem. Soc.* **1964**, *47*, 9.

(53) Stephen, M. *Angew. Chem., Int. Ed.* **2000**, *39*, 3392.

(54) Zhang, C.; Hou, Z.; Chai, R.; Cheng, Z.; Xu, Z.; Li, C.; Huang, L.; Lin, J. *J. Phys. Chem. C.* **2010**, *114*, 6928.

(55) Xu, Z.; Li, C.; Yang, D.; Wang, W.; Kang, X.; Shang, M.; Lin, J. *Phys. Chem. Chem. Phys.* **2010**, *12*, 11315.

(56) Wang, Z. L.; Hao, J. H.; Chan, H. L. W. *J. Mater. Chem.* **2010**, *20*, 3178.

(57) Aebischer, A.; Heer, S.; Biner, D.; Kramer, K.; Haase, M.; Gudel, H. U. *Chem. Phys. Lett.* **2005**, *407*, 124.

(58) Cao, Y.; Qin, W. P.; Zhang, J. S. *Opt. Commun.* **2010**, *283*, 547.

(59) Li, Z.; Zhang, Y. *Nanotechnology* **2008**, *19*, 345606.

(60) Boyer, J.-C.; Cuccia, L. A.; Capobianco, J. A. *Nano Lett.* **2007**, *7*, 847.

(61) Pichaandi, J.; van Veggel, F. C. J. M.; Raudsepp, M. *ACS Appl. Mater. Interfaces* **2009**, *2*, 157.

(62) Johnson, L. F.; Guggenheim, H. J.; Rich, T. C.; Ostermayer, F. W. *J. Appl. Phys.* **1972**, *43*, 1125.